

PCCP

Accepted Manuscript



This is an *Accepted Manuscript*, which has been through the Royal Society of Chemistry peer review process and has been accepted for publication.

Accepted Manuscripts are published online shortly after acceptance, before technical editing, formatting and proof reading. Using this free service, authors can make their results available to the community, in citable form, before we publish the edited article. We will replace this *Accepted Manuscript* with the edited and formatted *Advance Article* as soon as it is available.

You can find more information about *Accepted Manuscripts* in the [Information for Authors](#).

Please note that technical editing may introduce minor changes to the text and/or graphics, which may alter content. The journal's standard [Terms & Conditions](#) and the [Ethical guidelines](#) still apply. In no event shall the Royal Society of Chemistry be held responsible for any errors or omissions in this *Accepted Manuscript* or any consequences arising from the use of any information it contains.

**Synthesis, Characterization and
Photoinduced Charge Separation of
Carbon Nanohorn-Oligothiolenylenevinylene Hybrids†**

María Vizúete,^a María J. Gómez-Escalonilla,^a Myriam Barrejón,^a José Luis G. Fierro,^b
Minfang Zhang,^c Masako Yudasaka,^c Sumio Iijima,^{c,d} Pedro Atienzar,^c Hermenegildo
García^{c*} and Fernando Langa^{a*}

^a *Universidad de Castilla-La Mancha, Instituto de Nanociencia, Nanotecnología y
Materiales Moleculares (INAMOL), 45071, Toledo, Spain.*

E-mail: Fernando.Langa@uclm.es

^b *Instituto de Catálisis y Petroleoquímica, CSIC, Cantoblanco, 28049, Madrid, Spain.*

E-mail: jlgfierro@icp.csic.es

^c *Nanotube Research Center, National Institute of Advanced Industrial and Technology,
Higashi, Tsukuba, Ibaraki 305-8565, Japan.*

E-mail: m-yudasaka@aist.go.jp

^d *Department of Physics, Meijo University, Shiogamaguchi, Tenpakaku,
Nagoya 468-8502, Japan.*

^e *Instituto Universitario de Tecnología Química CSIC-UPV,
Universidad Politécnica de Valencia, 46022, Valencia, Spain.*

E-mail: hgarcia@gim.upv.es

Corresponding author

Fernando Langa de la Puente. E-mail: Fernando.Langa@uclm.es

ABSTRACT

The covalent coupling between oligo(thienylenevinylenes) (*n*TVs) and carbon nanohorns (CNHs) has been investigated. The resulting nanohybrids have been characterized by a combination of several techniques, including thermogravimetric analysis (TGA), X-ray photoelectron spectroscopy (XPS), high-resolution transmission electron microscopy (HR-TEM) and Raman spectroscopy. The photophysical properties of the new hybrids were investigated by steady-state and time-resolved spectroscopic techniques. A transient signal characterized by two kinetic regimes, one short decay within 0.5 μsec corresponding to around 80% of the total signal and another much longer-lived decay of 10 μsec , has been detected. The transient absorption spectra are characterized by a continuous absorption that increases in intensity towards shorter wavelengths, with a maximum at 430 nm. These transient signals have been assigned to the charge-separated state delocalized on CNHs based on the quenching behavior and by comparison with the photophysical properties of *n*TV in the absence and presence of quenchers. The photophysical behavior of covalent *n*TV-CNH conjugates with microsecond transients due to electrons and holes on CNHs contrasts with the absence of any transient for analogous *n*TV-C₆₀ conjugates, for which charge separation was not observed at timescales longer than nanoseconds. The photochemical behavior of CNHs is believed to derive from the amphoteric (electron donor and acceptor) properties of CNHs and from the larger number of carbon atoms (efficient delocalization) in CNHs compared with C₆₀.

1. INTRODUCTION

The long-term goal of applications in optoelectronic devices and light energy conversion¹⁻³ has led to a great deal of interest in the synthesis and characterization of modified carbon nanostructures containing covalently attached electron-donor or -acceptor unit.⁴⁻⁶ Considering that the extinction coefficients of most carbon nanostructures are low, conjugates in which a dye acts as a light harvester and as an electron-donor or -acceptor moiety have frequently been prepared. Among these dyes, both transition metal complexes, such as porphyrins and metal polypyridyl, and organic molecules that absorb visible light have been used to obtain covalently modified photoresponse carbon nanostructures.⁷⁻⁸

The chemical stability, good electron-donating properties and light absorption characteristics have led to the use of polythiophene and oligothiophenevinylene⁹⁻¹⁰ compounds for the preparation of modified carbon nanostructures including fullerenes, carbon nanotubes¹¹⁻¹⁴ and graphene.¹⁵

Oligo(thiophenevinylene)s (*n*TVs) are π -conjugated oligomers formed by a planar thiophene structure with vinylene connectors to provide the highest effective conjugation length and a narrow HOMO–LUMO gap.^{9,16}

Compared to carbon nanotubes (CNTs), carbon nanohorns (CNHs)¹⁷⁻¹⁹ are unique materials that contain sheath-like aggregates of graphene with lengths in the 50–100 nm range. CNHs are similar to carbon nanotubes but they are closed at one end with a conical cap and open at the other end. These nanostructures grow as spherical aggregates of graphene tubules and are produced in high yield and purity by CO₂ laser ablation of graphite in the absence of metal catalysts. Furthermore, in contrast to single-walled carbon nanotubes (SWCNTs), which can be metallic and semiconducting (a

disadvantage for electronic applications), *pristine* CNHs show semiconducting properties that make them very attractive for applications in nanotechnology.²⁰⁻²⁵

The morphology and dimensions of CNHs mean that they are generally difficult to suspend in a liquid phase, although physical and chemical treatment can remove smaller debris from these flower-like particles to give a material that can be suspended more easily in solvents like *N,N*-dimethylformamide (DMF) and water. In this regard, one topic of interest in this area is to highlight the possible differences in the activity and photophysical properties between CNHs and other carbon nanostructures due to the different morphologies and dimensions of these materials. Several strategies have been employed in an effort to obtain good dispersions. For example, the introduction of organic moieties onto the skeleton of CNHs has yielded soluble CNH-based materials.²⁶⁻²⁹ In the work described here, oligo(thiylenevinylenes) (*n*TVs) with different lengths ($n = 2, 4$) were employed as dyes to provide *modified* CNHs by covalent attachment.

The synthesis and characterization of two novel nanohybrids, **3** and **4**, that contain carbon nanohorns and oligothiylenevinylenes was carried out with the aim of characterizing their electron- or energy transfer-photoinduced processes. Evidence was found for the interaction between the ground and excited states of the oligothiylenevinylene moiety with CNHs, particularly in the context of related precedents in which similar systems had been attached to fullerene.¹⁴ Possible differences in these systems should serve to highlight the unique properties of CNHs when compared to fullerenes. Such specific behavior could be caused by the length of the CNHs allowing delocalization of electrons, which in turn would retard electron transfer in comparison to fullerene analogs. The amphoteric behavior of CNHs, *i.e.*, they act as electron acceptors and donors, contrasts with that of fullerenes and this

difference would allow the generation of much longer-lived charge-separated states in CNHs.

2. EXPERIMENTAL SECTION

2.1. Materials. CNHs were produced by CO₂ laser ablation of graphite in the absence of any metal catalyst under an argon atmosphere (760 Torr) at room temperature; the purity of the CNHs was as high as >90% for less amorphous carbons. All other chemicals used in the synthesis and spectroscopic measurements were purchased from Aldrich Chemicals (Milwaukee, WI) and were used as received.

2.2. General procedure

1,3-dipolar cycloaddition with thienylenevinylene oligomers: In a typical experiment, 50 mg of *pristine* CNHs were suspended in *N*-methyl-2-pyrrolidone (NMP) (100 mL) and dissolved with the aid of sonication for 10 min. Sarcosine and the corresponding thienylenevinylene oligomer were added portionwise every 24 h. The resulting mixture was heated for 4 days at 130 °C. The mixture was allowed to cool down to room temperature, filtered through a PTFE membrane (Millipore, 0.1 μm pore) and the solid was washed successively with DMF and CH₂Cl₂. The resulting black solid was purified by Soxhlet extraction with CH₂Cl₂ for 12 hours and the solvent was evaporated. A series of cycles of centrifugation-redispersion was then carried out with diethyl ether. The residue was dried overnight under vacuum to obtain the *functionalized* CNH material as a solid.

CNH-based material **3**

According to the general procedure, **3** was obtained from *pristine* CNHs (50 mg), NMP (100 mL), sarcosine (15 mg, 0.18 mmol, 4 eq) (3.75 mg every 24 hours) and (*E*)-1-(5-formyl-3,4-dihexyl-2-thienyl)-2-(3',4'-dibutyl-2'-thienyl)ethylene **5**³⁰ (25 mg, 0.045 mmol, 1 eq) (6.25 mg every 24 hours).

CNH-based material 4

According to the general procedure, **4** was obtained from *pristine* CNHs (50 mg), NMP (100 mL), sarcosine (15 mg, 0.18 mmol, 4 eq) (3.75 mg every 24 hours) and (*E,E,E*)-1,2-bis[5-(3',4'-dihexyl-2'-thienylvinyl)(3,4-dihexyl-2-thienyl)]ethylene **6**³⁰ (50 mg, 0.045 mmol, 1 eq) (12.5 mg every 24 h).

3. RESULTS AND DISCUSSION

The synthesis of formyl-oligothienylenevinylenes **5** and **6** was achieved by McMurry coupling reactions, as reported by Roncali *et al.*¹⁰ but with slight modifications.³⁰ The two new nanohybrids, CNH-2TV (**3**) and CNH-4TV (**4**), were prepared by 1,3-dipolar cycloaddition between aldehydes **5** or **6**, *N*-methylglycine and *pristine* CNH in NMP³¹ at 130 °C for 4 days (Scheme 1). The mixture was allowed to cool down to room temperature and the product was filtered off using a Millipore filter (0.1 µm PTFE membrane). The product was thoroughly washed several times with DMF and then with dichloromethane (CH₂Cl₂) (sonicated, centrifuged and filtered) until the filtrate remained colorless. The final purification of the materials was achieved by Soxhlet extraction in CH₂Cl₂ for 12 h. The Soxhlet extraction allowed the recovery of *functionalized* materials **3** and **4** from unreacted CNHs. Finally, the solvent was removed under reduced pressure to give the corresponding nanohybrid as a black solid.

The solubility of the resulting nanohybrid materials **3** and **4** allowed their characterization by Raman spectroscopy, TGA, XPS and high-resolution transmission electron microscopy (HR-TEM) to obtain detailed information about their structural and morphological properties. In addition, the electronic properties of the materials were explored by UV-vis absorption and steady-state and time-resolved spectroscopic

techniques. Finally, electrochemistry was employed to determine possible variations in the energy levels when photoactive units are grafted onto the CNH skeleton.

Raman spectroscopy provided significant evidence for the covalent grafting of the oligothiénylenevinylens onto the CNHs.³²⁻³³ The Raman spectrum of *pristine* CNH excited at 532 nm is shown in Fig. 1. The spectrum exhibits two prominent bands centered at $\sim 1600\text{ cm}^{-1}$ and $\sim 1350\text{ cm}^{-1}$ and these are, respectively, assigned to the G-band and the defect-induced D-band. It can be observed in Fig. 1a that the intensity of the D band of the *modified* CNHs **3** and **4** has an increased intensity and the I_D/I_G ratio changes from 1.06 for *pristine* CNHs to 1.71 for **3** and 1.25 for **4**. This increase in the I_D/I_G ratio upon functionalization is indicative of the incorporation of oligothiénylenevinylene units on the framework of the CNH. Another important feature of the Raman spectra is the existence of a peak at $\sim 2900\text{ cm}^{-1}$ (Fig. 1b) (denoted as the D+D' band), which is associated with the existence of defects and follows the trend of the D band.³³ Finally, a shift towards lower frequencies in the G band by $\sim 10\text{ cm}^{-1}$ was also observed when compared with *pristine* CNH (Fig. 1a). This change is the result of charge transfer, as occurs in systems doped with an electron donor moiety.³⁴⁻³⁶

The amount of organic mass covalently attached to the surface of the CNHs was quantified by thermogravimetric analysis³⁷ (TGA). It can be observed in Fig. S1, (see ESI†) that *pristine* CNH is thermally stable up to 800 °C but the traces corresponding to *functionalized* nanohybrids **3** and **4** show the most pronounced weight loss between 200 and 550 °C. This latter weight loss is attributed to the thermal decomposition of the organic units (2TV(**1**) and 4TV(**2**) respectively) attached to the CNH framework. In the case of nanohybrid **3**, the weight loss is 10% and this corresponds to one organic fragment grafted *per* 423 carbon atoms. This loss is comparable to that observed for the homologous hybrid **4** (9%), but in this case the weight loss corresponds to one

functional group covalently attached *per* 876 carbon atoms. The increase in the chain length in material **4** compared with **3** leads to a lower availability of π surface and this fact explains the lower degree of functionalization for **4**. This finding is in good agreement with the results observed in the Raman spectra (see Table S1).

X-ray photoelectron spectroscopy (XPS) was used in conjunction with Raman spectroscopy and TGA to confirm the presence of functional groups grafted to the surface of CNHs. The survey spectrum of the *pristine* CNHs (Fig. 2a) shows the predominant presence of carbon (96.1 at. %) and oxygen (3.9 at. %), thus demonstrating the high purity of the starting material. However, the XPS survey spectra of **3** and **4** (Figs. 3b and 3c) show the presence of all of the expected (sulfur and nitrogen) elements associated with the grafted materials, which supports the incorporation of the oligothiénylenevinylene units onto the CNH surface.

The high resolution XPS data for all of the materials were recorded and the corresponding binding energy values are collected in Table S2. All peaks were deconvoluted into several symmetrical components (i.e., five or six for C 1s; two for O 1s and one or two for N 1s). The C 1s peak of *pristine* CNH was satisfactorily fitted to five components (see ESI†, Fig. S2), according to the peak assignment used by Stankovich *et al.*³⁸ The most intense peak at 284.8 eV is due to sp^2 C–C bonds of graphitic carbon. The next three components at 286.3, 287.6 and 289.3 eV are often assigned to C–O, C=O and COO groups^{26,38-40} present on the surface of CNHs. Functionalized materials **3** and **4** display a sixth component at 285.4 eV (Fig. S3) due to sp^3 C–C bonds, corresponding to the alkyl chain of thienylenevinylene fragments.⁴¹ In addition, all samples displayed a weak component at around 291.4 eV and this corresponds to a π - π^* transition of C atoms in graphene structures.³⁹

Analysis of the O 1s peak for *pristine* CNHs and **3** and **4** was resolved with two components of almost the same intensity (see ESI†, Table S2). For the starting material, the first component at 532.2 eV corresponds to O=C surface groups and the second one, at 533.5 eV, is often associated with O–C bonds.^{42,43} These observations are consistent with the existence of oxygen functional groups on the CNH surface. The same components were observed for **3** and **4**, although both components are slightly shifted toward lower binding energies (Table S2).

The presence of N atoms in compounds **3** and **4** confirmed that the CNHs had been functionalized. The high-resolution N1s peak of hybrid **3** is shown in Fig. S4a. It can be seen that there is a single component at a binding energy of 400.3 eV, which belongs to an N-atom bound to a C-atom as the nearest neighbor. This atom is assigned to the pyrrolidine ring.⁴⁴ In addition, the S 2p peak for **3** (see Fig. S5a) recorded under high resolution conditions allowed detection of the two components of the doublet (S2p_{3/2}-2p_{1/2}), with the most intense one at 164.1 eV. This binding energy is characteristic of the S–C bond of thiophene-like compounds.^{45,46} The same components were also detected in the case of **4** (see Figs. S4b and S5b).

XPS was also used to quantify the proportions of the elements on the surface. The fitted peak areas were used as relative intensities and the appropriate relative sensitivity factors for C 1s (0.25), N 1s (0.42) and O 1s (0.66)⁴⁷ were applied to estimate the relative chemical composition of all samples. The data are collected in Table 1. In hybrids **3** and **4** the experimental atomic S/N ratios of 1.91 and 3.78, respectively, are very similar to the theoretical stoichiometric values for **2** and **4**, according to Scheme 1. This result provides conclusive evidence that the oligothiénylvinylene moieties had been attached on the CNH substrate.

The morphologies of hybrids **3** and **4** were evaluated by high-resolution transmission electron microscopy (HR-TEM). The spherical aggregate form of CNHs was maintained in **3** and **4** (Figs. 3a and 3c). The magnified images showed some material attached to the CNH surfaces (Figs. 3b and 3d) and this could be attributed to the conjugated moieties.

The good solubility of the *functionalized* CNHs **3** and **4** allowed their characterization by spectroscopic techniques. The UV-vis spectra of **3** and **4** (Fig. 4) exhibit the characteristic absorption band of the oligothiophenevinylene unit and this the covalent functionalization of the CNH.

In order to study intrahybrid interactions that may take place between the oligothiophenevinylene moiety and the CNH in nanohybrids **3** and **4**, electrochemical measurements and fluorescence emission spectroscopy were carried out on solutions in DMF at room temperature.

Electrochemical studies using Osteryoung square wave voltammetry (OSWV) were performed in an effort to understand the redox behavior of CNH-*n*TV hybrids **3** and **4** and comparisons were made with non-functionalized *n*TVs **1** and **2** (see Scheme S1 in ESI†). On the anodic side, **3** and **4** revealed two oxidation peaks (**3**: +0.69 V and +1.01 V; **4**: +0.28 V and +0.45 V) and these were shifted to higher potentials with respect to model compounds **1** and **2** when measured under identical conditions (**1**: +0.44 V and +0.77 V; **2**: +0.16 V and +0.35 V) (see Fig. S6 and Table S3 in ESI†).

The greater difficulty in oxidizing *n*TV oligomers when they are covalently linked to the CNH indicates the existence of electronic communication in the ground state between the conjugated thiophenevinylene oligomers as electron donors and CNHs as electron acceptors. Thus, the electrochemistry, and specifically the increase in the

oxidation potentials, points to an incipient electron donation from the conjugated agent to the CNH scaffold. This variation in the oxidation potential of the *n*TV moiety depending on the covalent attachment to CNHs is in contrast to the reported lack of influence on the oxidation potential of this electron donor moiety covalently bonded to fullerene.¹⁴ It is possible that the planar graphene wall of CNHs allows better interaction between *n*TV moieties and the CNH in comparison to the spherical fullerenes. In the case of nanohybrid **3** (Fig. 5, left), photoexcitation at 405 nm led to substantial quenching of the oligothiénylenevinylene emission band. In the case of nanohybrid **4** (Fig. 5, right), no emission was observed upon 489 nm excitation, indicating that for this nanohybrid the excited state of 4TV is quenched intramolecularly by CNH. These observations strongly support electronic interactions between the oligothiénylenevinylene units and CNH in the excited state.

In an effort to gain an insight in the photophysics of nanohybrids **3** and **4**, transient absorption spectroscopy was carried out on dyes **1** (2TV) and **2** (4TV) (see Scheme S1 in ESI) in polar solvents in the absence and presence of quenchers using 355 nm laser excitation. These studies should provide information about the nature of the transient species generated upon excitation of these organic dyes and could also elucidate their possible interaction with CNHs. It was envisaged that the data would be useful at a later stage to rationalize the photochemical behavior of the conjugates **3** and **4**.

Laser excitation of **1** at 355 nm gave rise to a short-lived transient species that decayed completely on the microsecond timescale. The transient spectra recorded for **1** are characterized by a sharp, intense absorption peak at λ_{max} 430 nm accompanied by a much less intense broad absorption from 500 to 650 nm (see Fig. 6). This transient was completely quenched by oxygen but not by N₂O. This quenching behavior, together

with the short lifetime, is compatible with the assignment of the transient to a triplet excited state of **1**. The addition of methyl viologen (MV^{2+}) led to the gradual replacement of the **1** triplet transient by the MV^{2+} radical cation, which was characterized by the typical MV^{+} spectrum with a sharp peak at 390 nm and a less intense broad band from 500 to 700 nm. In addition, the triplet excited state of **1** was also quenched by methanol but in this case, since the CH_3O^+H radical cation cannot be detected, the only observation was the quenching of the triplet signal of **1** accompanied by hydrogen generation as detected by GC analysis of the gas phase. In fact methanol is widely used as sacrificial electron donor in photocatalytic hydrogen generation.^{48,49} This behavior indicates that the triplet excited state of **1** can act as an electron donor or acceptor depending on the nature of the quencher, as indicated in Scheme 2.

Convincing evidence in support of the occurrence of photoinduced electron transfer was visually observed by performing steady state lamp irradiation of mixtures of **1** (2TV) and CNHs in DMF solvent containing methanol as hole quencher and MV^{2+} as electron acceptor, where by formation of blue color was observed by naked eyes. Control experiments irradiating in DMF, MV^{2+} and methanol did not lead to any blue coloration. At the end of the experiment a change in the steady state UV-vis absorption spectrum exhibiting a new peak at 460 nm was recorded (see ESI, Figure S7-left). Analogous experiments in which nanohybrid **4** was irradiated in DMF containing MV^{2+} and MeOH also lead to the development of blue color and, even more, in this case steady state UV-vis absorption spectrum of the solution allow to detect the presence of some residual MV^{+} radical cation (see ESI, Figure S7-right).

The addition of CNHs as quencher led to gradual changes in the transient absorption spectrum of **1**, which was characteristic of the triplet excited state, to give a different transient absorption spectrum characterized by a continuous absorption in the

whole spectral range (Fig. 7). This quenching study provides evidence that the triplet excited state of compound **1** is intercepted by CNHs as quencher and that a new species corresponding to the charge separated state is generated. According to the Scheme 2, for the **1**/CNH mixture, excitation of **1** and generation of the triplet excited state will be followed by electron donation from $\mathbf{1}^3$ to CNHs. Evidence in support of this proposal has been provided above when commenting the photophysical behavior of mixtures of **5** and CNH and nanohybrid **3** in the presence of MV^{2+} .

Further evidence for the quenching of the electronic excited state of dye **1** by CNHs was obtained by femtosecond transient spectroscopy on monitoring the singlet excited state. Laser excitation at 400 nm led to the instantaneous generation of a transient absorption characterized by the growth of a band from 450 to 700 nm, which peaked at 620 nm (Fig. 8). Addition of CNHs led to an increase in the decay rate constant of the singlet excited state (see inset in Fig. 8), which indicates that the singlet excited state is also quenched by CNHs.

An analogous study was performed on compound **2** (4TV) in DMF solution, unfortunately no femtosecond triplet signal could be observed for compound **2**, probably due to insufficient concentration of this compound. Typically femtosecond transient experiments requires highly concentrated solutions that were not possible to reach for compound **2**. For this organic dye, 355 nm nanosecond laser excitation generated an absorption band that spanned the range from 450 to 700 nm. The lifetime of this band was much longer than that of **1** (compare decays in Figures 6 and 9 for the lifetimes of transients from **1** and **2**, respectively). This transient decay on the microsecond timescale was also assigned to a triplet excited state of **2** due to quenching by oxygen, although this state was not sensitive to the presence of N_2O (see Fig. 9, left inset). In a similar way to **1**, the triplet excited state of **2** was also quenched by MV^{++} as

an electron acceptor and MeOH as an electron donor to give rise rapidly to 2^{+} or 2^{-} , respectively. On using MV^{++} as the quencher, the growth of the signal at 400 nm was attributed to the generation of the MV^{+} radical cation formed simultaneously with the disappearance of the triplet excited state of **2**. As in the case of **1**, the presence of CNHs as a quencher in conjunction with compound **2** led to changes in the temporal profile of the signal and in the intensity of the band corresponding to the triplet excited state of **2**. It can be seen from Fig. 10 how the presence of CNHs led to a considerable decrease in the intensity of the ΔOD value and also to changes in the kinetics of the signal.

In summary, transient spectroscopy showed that upon excitation dyes **1** and **2** generated the corresponding triplet state and this can undergo electron transfer quenching depending on the nature of the quencher. In the case of dye **1**, femtosecond laser studies showed that the singlet excited state is also quenched by CNHs.

Laser flash photolysis experiments on nanohybrids **3** and **4** were also carried out with excitation at 355 nm. Supporting information (Figures S8-S10) contains also the transient absorption spectra recorded for nanohybrid **4**, the larger conjugation of the oligothiophenevinylene covalently should allow also excitation at larger wavelength such as 532 nm. However, since coincident transient absorption spectra and temporal signal profile were obtained for nanohybrid **4**. Using either 355 or 532 nm, only the former excitation wavelength will be commented. Reader is referred to the supporting information for 532 laser data. According to the absorption spectra of the individual components (see Fig. 4), this wavelength should mainly produce excitation of the CNHs and minimize the influence of the variation of the absorption spectrum on moving from dye **1** to dye **2**.

Laser excitation at 355 nm gave rise to transient spectra that decayed in a few microseconds for both nanohybrids **3** and **4**. Selected transient spectra recorded for

these two CNH conjugates **3** and **4** are shown in Fig. 11. It can be seen that the transient spectra for the two modified CNHs **3** and **4** are similar and are characterized by a continuous absorption in the 380 to 800 nm region. This absorption decreases gradually in intensity at longer wavelengths and has a relative absorption maximum at 430 nm. The transient spectra resemble the ground state UV-vis absorption spectra of the **3** and **4** constructs, in which the CNH contribution predominates and the defined absorption bands of the thienylvinylenes moieties are barely visible (compare spectra in Figs. 4 and 11). The transient absorption spectra recorded upon photolysis of **3** and **4** conjugates are remarkably similar to that presented in Fig. 7 for the transient spectra upon quenching of the triplet state of **1** by CNH (compare Figs. 7b and 11). Given the similarities in the transient absorption spectra of conjugates **3** and **4** and the absorption spectra of the CNH ground state, we attribute these transient species to the charge-separated state (electron and holes) located on CNH components. The temporal profile of the signal was very similar over the whole spectral window and two decays were evident (the temporal profiles of the signals at two representative wavelengths are shown in the insets in Fig. 11). The fast decay regime corresponds to about 50% or 80% of the signal for **3** and **4**, respectively, and this process was too fast to be monitored in our nanosecond laser system as it was complete within about 500 ns after the laser pulse. Although the laser pulse was only 7 ns fwhm, the temporal profile response of the system was much slower due to the limitation of the detector and photomultiplier caused by light scattering of the nanohybrid dispersion in DMF. The residual signal after 500 ns was less intense for **3** and the decay was slower than for **4**.

Assignment of this residual signal to a charge separated state was also supported by quenching studies with electron-acceptor and -donor compounds. Time-resolved absorption spectra recorded in the presence of some of the quenchers used in the present

study are shown in Fig. 12. For example, the presence of oxygen quenches the signal completely – even the faster component. Methanol is a typical hole quencher and this also accelerated the kinetics of the decay for nano hybrids **3** and **4**, although for this quencher some variation in the quenching constants were observed depending on the monitored wavelength. In this way, methanol as a quencher has a more marked influence on the 400 to 600 nm region than on the 600 to 800 nm region. This fact is not surprising given that the overall signal should be a combination of electrons and holes and the independent contribution of these two components could be different depending on the monitored wavelength. Similarly, N₂O, an electron quencher, also increased the decay kinetics for conjugate **4**. In the case of N₂O quenching of the **4** transient significant differences were observed in the 400–500 nm and 500–800 nm regions for N₂O quenching. In the 400–500 nm region, the transient signal of **3** underwent quenching with a decreasing lifetime of the kinetic components and this decayed in the microsecond timescale. In the 500–800 nm region, however, this residual signal was longer lived. Overall, the influence of quenchers on the transient spectra of **3** and **4** supports the assignment of the microsecond transient signal for modified CNHs **3** and **4** to a charge separated state. On the basis of the time-resolved spectroscopic data, the mechanism presented in Scheme 3 can be proposed for the photophysics of conjugates **3** and **4** (see Scheme 3). It is worth noting that **1**^{•+} and **2**^{•+} should have weak absorption spectra since a band attributable to the *n*TV^{•+} radical cation was not observed in the preliminary studies on the photolysis of **3** and **4** and quenching of the corresponding ³**1**^{*} and ³**2**^{*} triplet excited state by MV^{•+}. These characteristics suggest that the transient being monitored in the microsecond timescale arises from delocalization of charge carriers of CNHs (Scheme 3). The proposal of two types of positive holes, either trapped on *n*TV or freely moving on CNHs is compatible with the temporal profiles of

the transient signal showing two regimes, one shorter than 500 ns, attributable to the initial charge separation state and a longer lived state after migration of the positive holes. The summary of the major transient absorption measurements characteristics are: i) the short (sub-microsecond) lifetime of the excited state of **1** determined by femtosecond transient absorption spectroscopy, ii) the absence of an absorption band attributable to any of the reported *n*TV transient species and also iii) the broad continuous absorption characteristic of charge carriers on graphenes.

4. CONCLUSIONS

In this work, we present the covalent attachment of oligothiophenevinylene moieties to CNH. The transient species observed upon excitation at 355 nm for these nanoensemble *n*TV-CNHs are consistent with the generation of charge-separated states. Comparison of the transient spectra of *n*TV-CNH conjugates **3** and **4** with those recorded for compounds **1** and **2** rules out the presence of triplets **1** or **2** in the transient spectra of nanohybrids **3** and **4**. The quenching behavior of dye **1** in the singlet and triplet excited states and dye **2** in the triplet state by CNHs also provide evidence of a photoinduced electron transfer between the two components even in the absence of covalent attachment. The behavior of conjugates **3** and **4** contrasts with that of analogous *n*TV-C₆₀ conjugates, for which a charge separation transient was not observed on the nanosecond timescale. This contrasting behavior illustrates the advantages of CNHs as scaffolds, when compared with fullerenes, derived from the amphoteric (electron donor and acceptor) behavior of CNHs and the increased length of CNHs when compared to fullerenes.

ACKNOWLEDGMENTS

Financial support from the Spanish Ministry of Economy and Competitiveness (Severo Ochoa, CTQ2011-26455, CTQ2012-32315 and CTQ2013-48252-P) and Junta de

Comunidades de Castilla-La Mancha (PEII-2014-014-P) is gratefully acknowledged. P.A. also thanks the Spanish Ministry of Science and Innovation for a Ramon y Cajal research associate contract (RYC-2012-10702) and the Generalitat Valenciana for the grant GV-2014/101. M.B. thanks the MINECO for a doctoral FPI grant. We also acknowledge M. C. Cuquerella for performing the femtosecond spectroscopy measurements

†**Electronic supplementary information (ESI) available:** TGA, XPS spectra, electrochemistry data and absorption and transient spectra data.

REFERENCES

- 1 N. Aich, J. Plazas-Tuttle, J. R. Lead and N. B. Saleh, *Environ. Chem.*, 2014, **11**, 609-623.
- 2 M. F. L. De Volder, S. H. Tawfick, R. H. Baughman and A. J. Hart, *Science*, 2013, **339**, 535-539.
- 3 J. M. Schnorr and T. M. Swager, *Chem. Mater.*, 2011, **23**, 646-657.
- 4 N. Karousis and N. Tagmatarchis, *Chem. Rev.*, 2010, **110**, 5366-5397.
- 5 *Carbon Nanotubes and Related Structures: Synthesis, Characterization, Functionalization, and Applications*, ed. D. M. Guldi and N. Martín, Wiley-VCH Verlag GmbH & Co. Kga, 2010.
- 6 V. Georgakilas, J. A. Perman, J. Tucek and R. Zboril, *Chem. Rev.*, 2015, **115**, 4744-4822.
- 7 G. Bottari, G. de la Torre and T. Torres, *Acc. Chem. Research.*, 2015, **48**, 900-910.
- 8 T. Hasobe, *J. Phys. Chem. Lett.*, 2013, **4**, 1771-1780.
- 9 J. Roncali, *Acc. Chem. Res.*, 2000, **33**, 147-156.
- 10 I. Jestin, P. Frere, N. Mercier, E. Levillain, D. Stievenard and J. Roncali, *J. Am. Chem. Soc.*, 1998, **120**, 8150-8158.

- 11 F. Oswald, D.-M. Shafiqul Islam, M. E. El-Khouly, Y. Araki, R. Caballero, P. de la Cruz, O. Ito and F. Langa, *Phys Chem Chem Phys*, 2014, **16**, 2443-2451.
- 12 F. Oswald, D.-M. S. Islam, Y. Araki, V. Troiani, P. de la Cruz, A. Moreno, O. Ito and F. Langa, *Chem.-Eur. J.*, 2007, **13**, 3924-3933.
- 13 F. Oswald, D. M. S. Islam, Y. Araki, V. Troiani, R. Caballero, P. de la Cruz, A. Moreno, O. Ito and F. Langa, *Chem. Commun.*, 2007, 4498–4500.
- 14 J. J. Apperloo, C. Martineau, P. A. van Hal, J. Roncali and R. A. J. Janssen, *J. Phys. Chem. A*, 2002, **106**, 21-31.
- 15 Y. S. Liu, J. Y. Zhou, X. L. Zhang, Z. B. Liu, X. J. Wan, J. G. Tian, T. Wang and Y. S. Liu, *Carbon*, 2009, **47**, 3113-3121.
- 16 I. Jestin, P. Frère, P. Blanchard and J. Roncali, *Angew. Chem., Int. Ed.*, 1998, **37**, 942-945.
- 17 S. Zhu and G. Xu, *Nanoscale*, 2010, **2**, 2538-2549.
- 18 K. Pramoda, K. Moses, M. Ikram, K. Vasu, A. Govindaraj and C. N. R. Rao, *J. Clus. Sci.*, 2014, **25**, 173-188.
- 19 G. Pagona and N. Tagmatarchis, in *Advances in Carbon Nanomaterials: Science and Applications: Carbon Nanohorns Chemical Functionalization*, ed. N. Tagmatarchis, Pan Stanford Publishing, 1st edn, ch. 6, pp. 239–268, 2012.
- 20 S. Cataldo, P. Salice, E. Menna and B. Pignataro, *Energy Environ. Sci.*, 2012, **5**, 5919-5940.
- 21 G. Pagona, G. E. Zervaki, A. S. D. Sandanayaka, O. Ito, G. Charalambidis, T. Hasobe, A. G. Coutsolelos and N. Tagmatarchis, *J. Phys. Chem. C*, 2012, **116**, 9439-9449.

- 22 R. D. Costa, S. Feihl, A. Kahnt, S. Gambhir, D. L. Officer, G. G. Wallace, M. I. Lucio, M. A. Herrero, E. Vázquez, Syrgiannis, Z. M. Prato and D. M. Guldi, *Adv. Mater.*, 2013, **25**, 6513-6518.
- 23 Q. Zhang, J. Q. Huang, W. Z. Qian, Y. Y. Zhang and F. Wei, *Small*, 2013, **9**, 1237-1265.
- 24 F. Lodermeier, R. D. Costa, R. Casillas, F. T. U. Kohler, P. Wasserscheid, M. Prato, and D. M. Guldi, *Energy Environ. Sci.*, 2015, **8**, 241-246.
- 25 M. Vizueté, M. J. Gómez-Escalonilla, J. L. G. Fierro, A. S. D. Sandanayaka, T. Hasobe, M. Yudasaka, S. Iijima, O. Ito and F. Langa, *Chem.–Eur. J.*, 2010, **16**, 10752-10763.
- 26 M. Vizueté, M. J. Gómez-Escalonilla, J. L. García-Fierro, M. Yudasaka, S. Iijima, M. Vartanian, J. Iehl, J-F. Nierengarten, F. Langa, *Chem. Commun.*, 2011, **47**, 12771-12773.
- 27 G. Pagona, N. Karousis and N. Tagmatarchis, *Chem. Phys. Lett.*, 2011, **516**, 76-81.
- 28 G. Pagona, G. Rotas, I. D. Petsalakis, G. Theodorakopoulos, A. Maigné, J. Fan, M. Yudasaka, S. Iijima and N. Tagmatarchis, *J. Nanosci. Nanotechnol.*, 2007, **7**, 3468-3472.
- 29 G. Pagona, N. Karousis and N. Tagmatarchis, *Carbon*, 2008, **46**, 604–610.
- 30 M. Urbani, B. Pelado, P. de la Cruz, K. Yamanaka, O. Ito and F. Langa, *Chem.- Eur. J.*, 2011, **17**, 5432-5444.
- 31 C. Cioffi, S. Campidelli, F. G. Brunetti, M. Meneghetti and M. Prato, *Chem. Comm.*, 2006, 2129-2131.
- 32 S. Utsumi, H. Honda, Y. Hattori, H. Kanoh, K. Takahashi, H. Sakai, M. Abe, M. Yudasaka, S. Iijima and K. Kaneko, *J. Phys. Chem. C*, 2007, **111**, 5572-5575.
- 33 C. Fantini, M. A. Pimenta and M. S. Strano, *J. Phys. Chem. C*, 2008, **112**, 13150-13155.

- 34 R. Voggu, C. S. Rout, A. D. Franklin, T. S. Fisher and C. N. R. Rao, *J. Phys. Chem. C*, 2008, **112**, 13053-13056.
- 35 G. M. Do Nascimento, T. Hou, Y. A. Kim, H. Muramatsu, T. Hayashi, M. Endo, N. Akuzawa and M. S. Dresselhaus, *Carbon*, 2011, **49**, 3585-3596.
- 36 J. Y. Mevellec, C. Bergeret, J. Cousseau, J. P. Buisson, C.P. Ewels and S. Lefrant, *J. Am. Chem. Soc.*, 2011, **133**, 16938-46.
- 37 C. Herrero-Latorre, J. Álvarez-Méndez, J. Barciela-García, S. García-Martín and R. M. Peña-Crecente, *Analytica Chimica Acta*, 2015, **853**, 77-94 and references herein.
- 38 S. Stankovich, D. A. Dikin, R. D. Piner, K. A. Kohlhaas, A. Kleinhammes, Y. Jia, Y. Wu, S. T. Nguyen and R. S. Ruoff, *Carbon* 2007, **45**, 1558-1565.
- 39 E. Bekyarova, M. E. Itkis, P. Ramesh, C. Berger, M. Sprinkle, W. A. de Heer and R. C. Haddon, *J. Am. Chem. Soc.*, 2009, **131**, 1336-1337.
- 40 M. Barrejón, S. Pla, I. Berlanga, M. J. Gómez-Escalonilla, L. Martín-Gomis, J. L. G. Fierro, M. Zhang, M. Yudasaka, S. Iijima, H. B. Gobeze, F. D'Souza, A. Sastre-Santos and F. Langa, *J. Mater. Chem. C*, 2015, **3**, 4960-4969.
- 41 A. Criado, M. Vizuete, M. J. Gómez-Escalonilla, S. García-Rodríguez, J. L. García Fierro, A. Cobas, D. Peña, E. Guitián and F.Langa, *Carbon*, 2013, **63**, 140-148.
- 42 M. J. Gómez-Escalonilla, P. Atienzar, J. L. G. Fierro, H. García and F.Langa, *J. Mater. Chem.*, 2008, **18**, 1592-1600 and references therein.
- 43 E. del Campo, K. Flavin, D. Movia, C. Navio, C. Bittencourt and S. Giordani, *Chem. Mater.*, 2011, **23**, 67-64 and references therein.
- 44 S. Giordani, J-F. Colomerc, F. Cattaruzza, J. Alfonsid, M. Meneghetti, M. Prato and D. Bonifazi, *Carbon*, 2009, **47**, 578-588.
- 45 M. Hahlin, E. M. J. Johansson, S. Plogmaker, M. Odelius, D. P. Hagberg, L. Sun, H. Siegbahn and H. Rensmo, *Phys. Chem. Chem. Phys.*, 2010, **12**, 1507-1517S.

46 V. Kamat, J. B. Yadav, V. Puri, R. K. Puri and O. S. Joo, *Appl. Surface Sci.*, 2011, **258**, 482-488.

47 C. D. Wagner, L. E. Davis, M. V. Zeller, J. A. Taylor, R. H. Raymond and L.H. Gale, *Surf. Interface Anal.*, 1981, **3**, 211-221.

48 P. Cuendet, K.K. Rao, M. Grätzel and D.O. Hall, *Biochimie*, 1986, **1**, 217-221.

49 J. Soldat, R. Marschall and M. Wark, *Chem. Sci.*, 2014, **5**, 3746-3752

Captions of figures, tables and schemes.

Scheme 1. Schematic illustration for the preparation of CNH-based materials **3** and **4**.

Scheme 2. Proposed photochemistry of **1** after 355 nm laser excitation and with MV^{++} or MeOH as electron-acceptor or -donor quenchers, respectively.

Scheme 3. Mechanism proposed for the photochemistry of *n*TV-CNH nanohybrids after 355 nm laser excitation (CS: charge separation).

Table 1 Chemical composition measured by XPS.

Fig. 1. (a) Raman spectra obtained upon excitation at 532 nm of *pristine* CNHs (black) and *modified* CNHs **3** (red) and **4** (blue). The spectra are normalized to the peak intensity of the G band, (b) detail of the G' and D+D' region.

Fig. 2. XPS survey spectra of (a) *pristine* CNH, (b) **3** and (c) **4**.

Fig. 3. HR-TEM images of CNH-2TV (**3**) (a, b) and CNH-4TV (**4**) (c, d).

Fig. 4. Absorption spectra of *pristine* CNH (gray), free oligothiolenylenevinylenes **5** and **6** (dotted line) and *functionalized* CNHs **3** and **4** (solid line), measured in DMF.

Fig. 5. Fluorescence spectra recorded in DMF of (left) **5** (dotted line) and *functionalized* CNH **3** (solid line), excitation at 405 nm; (right) **6** (dotted line) and *functionalized* CNH **4** (solid line), excitation at 489 nm.

Fig. 6. Transient spectra recorded at 40 ns after 355 nm laser excitation of an Ar-purged DMF solution of 2.6×10^{-5} M **1** before (a) and after (b) the addition of 50 μ L of a DMF solution of MV^{++} ($MVCl_2$, 0.01 M). The inset shows the signal decay monitored at 420 nm on purging with Ar, O_2 or N_2O and after the addition of 100 μ L of MeOH as an electron donor or 50 μ L of a DMF solution of $MVCl_2$ (0.01 M) as an electron acceptor.

Fig. 7. Transient spectra recorded at 40 ns after 355 nm laser excitation of an Ar-purged DMF solution of 2.6×10^{-5} M **1** before (a) and after (b) the addition of 50 μ L of a DMF

solution of CNHs (0.2 mg/mL). The inset shows the comparative signal decay monitored at 420 nm before (a) and after (b) the addition of the CNH solution.

Fig. 8. Femtosecond transient spectra recorded from 1.78 to 150 ps after 400 nm laser excitation of an Ar-purged DMF solution of **1** (2.6×10^{-4} M). The inset shows the comparative signal decay monitored at 625 nm before (a) and after (b) the addition of a DMF solution of CNHs (0.2 mg/mL).

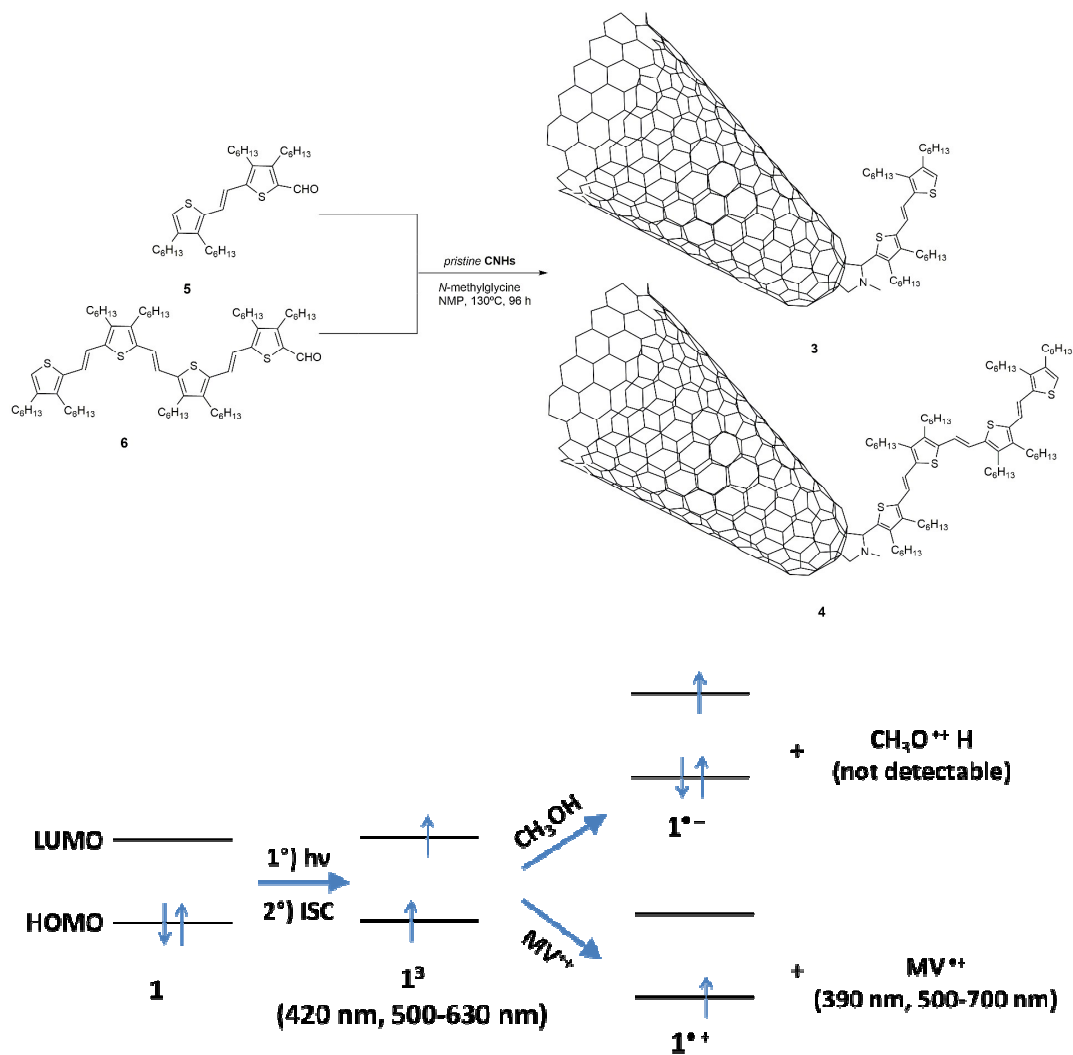
Fig. 9. Transient spectra recorded 7 μ sec after 355 nm laser excitation of an Ar-purged DMF solution of 4.5×10^{-5} M **2** before (a) and after (b) the addition of 50 μ L of a DMF solution of MV^{++} ($MVCl_2$, 0.01 M). The left inset shows the signal decay monitored at 420 nm on purging with Ar, O_2 or N_2O and after the addition of 100 μ L of MeOH as an electron donor or 50 μ L of a DMF solution of $MVCl_2$ (0.01 M) as an electron acceptor. The right inset shows the signal decay monitored at 550 nm on purging with Ar (a) and after the addition of 50 μ L of a DMF solution of $MVCl_2$ (0.01 M) (b).

Fig. 10. Transient spectra recorded 0.45 μ sec after 355 nm laser excitation of an Ar-purged DMF solution of 4.5×10^{-5} M **2** before (a) and after (b) the addition of 50 μ L of a DMF solution of CNH (0.2 mg/mL). The inset shows the comparative signal decay monitored at 550 nm before (a) and after (b) addition of the CNH solution.

Fig. 11. Transient spectra recorded from 51 ns to 0.45 μ s after 355 nm laser excitation of an Ar-purged DMF solution of nanohybrid **3** (a) and **4** (b). The temporal profiles of the transient signal monitored at 420 (a) and 550 nm (b) of Ar-purged solutions of **3** (A) (inset in a) and **4** (B) (inset in b).

Fig. 12. Comparative transient spectra recorded at 50 ns after 355 nm laser excitation of a DMF solution of (a) nanohybrid **3** and (b) nanohybrid **4** after purging with Ar, O_2 , N_2O and addition of 100 μ L of MeOH.

Scheme 1. Scheme 2.



Scheme 3.

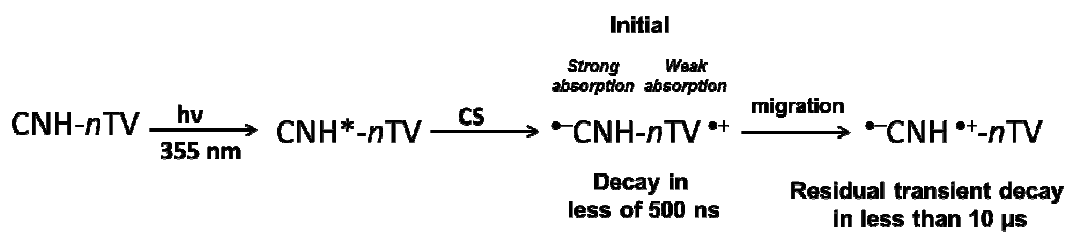


Table 1

Sample	C (% at)	O (% at)	N (% at)	S (% at)
<i>pristine CNHs</i>	96.1	3.9	-	-
3	92.1	4.7	1.1	2.1
4	90.7	5.0	0.9	3.4

Fig. 1.

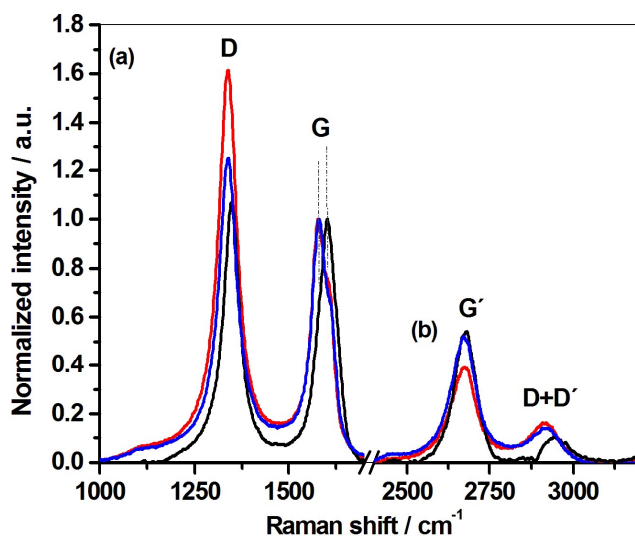


Fig. 2.

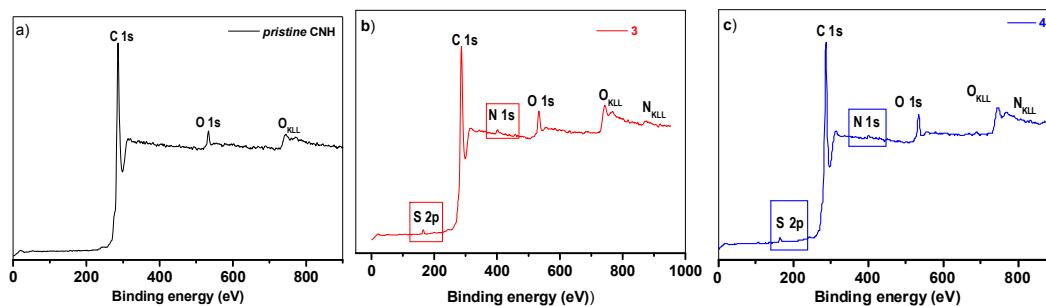


Fig. 3.

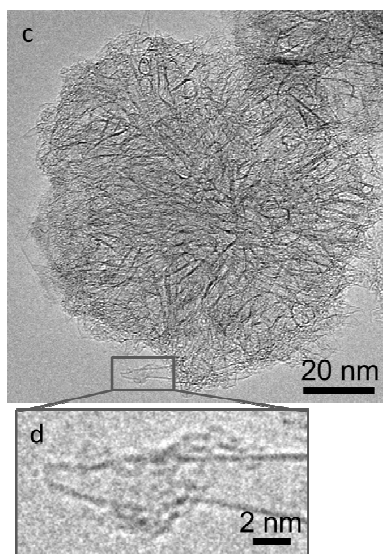
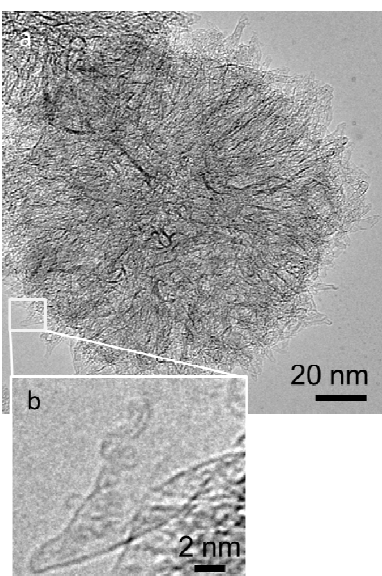


Fig. 4.

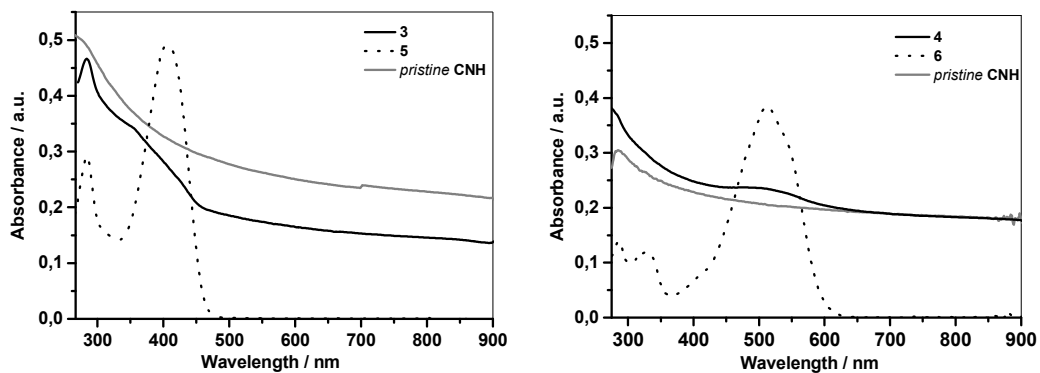


Fig. 5.

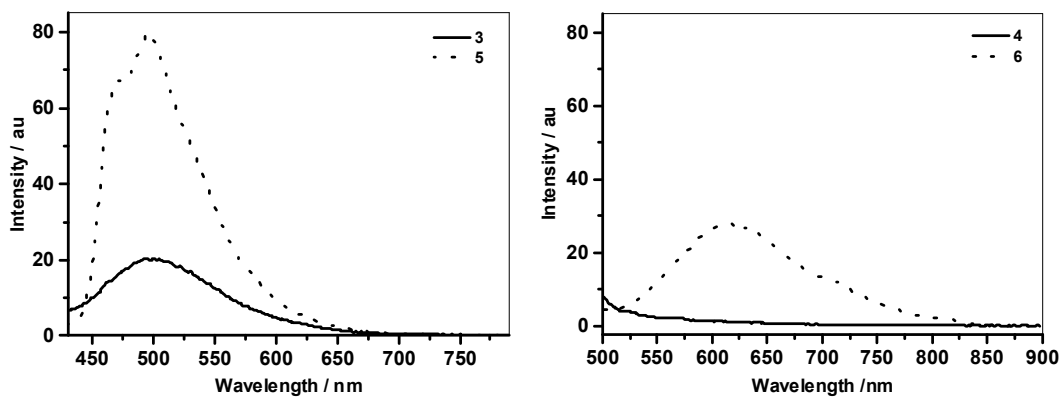


Fig. 6.

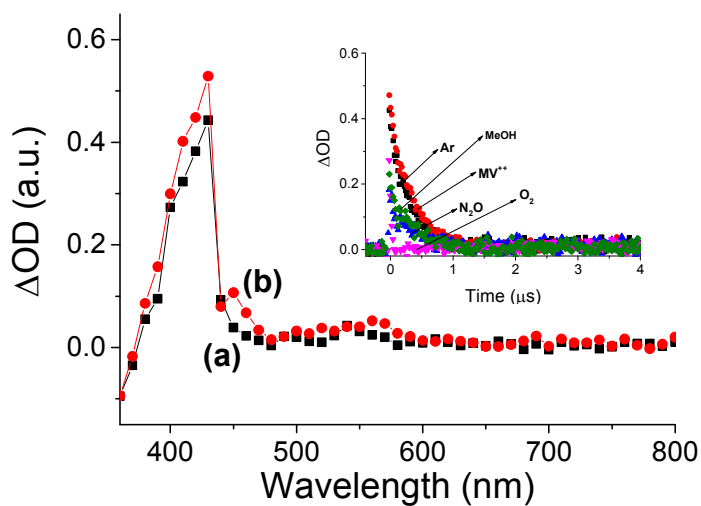


Fig. 7.

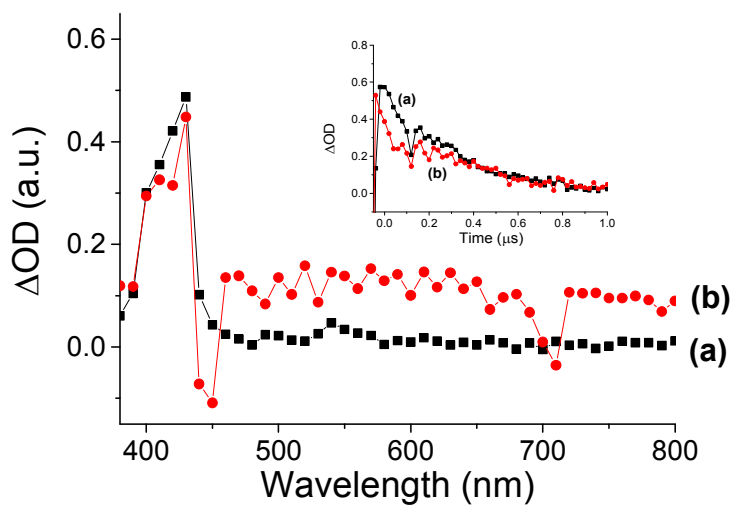


Fig. 8.

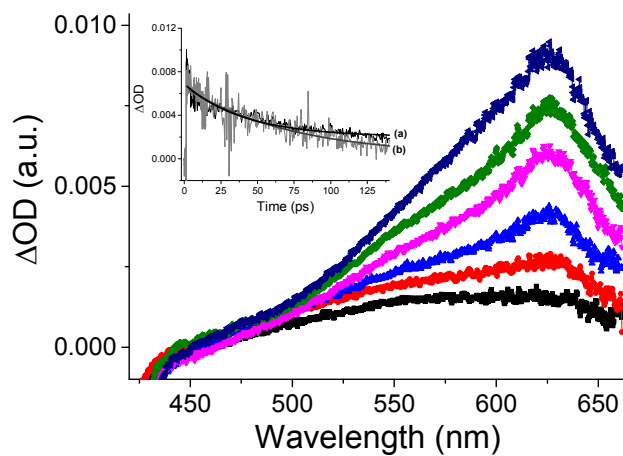


Fig. 9.

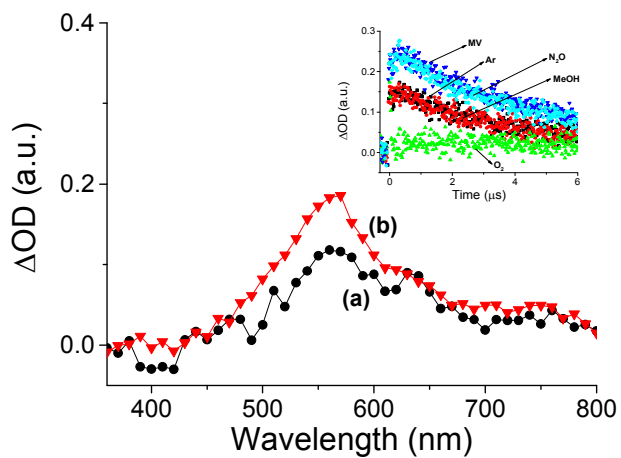


Fig. 10.

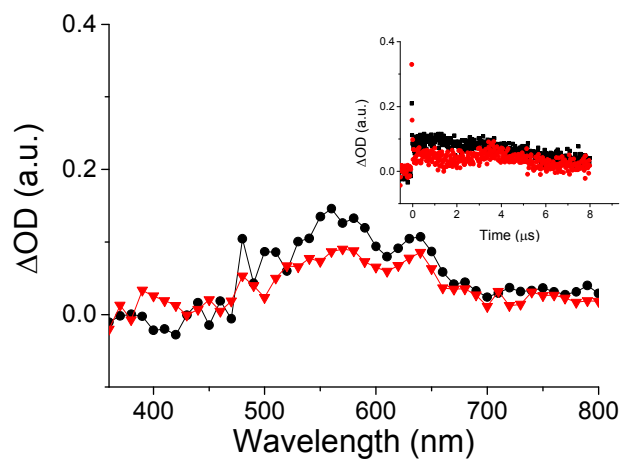


Fig. 11.

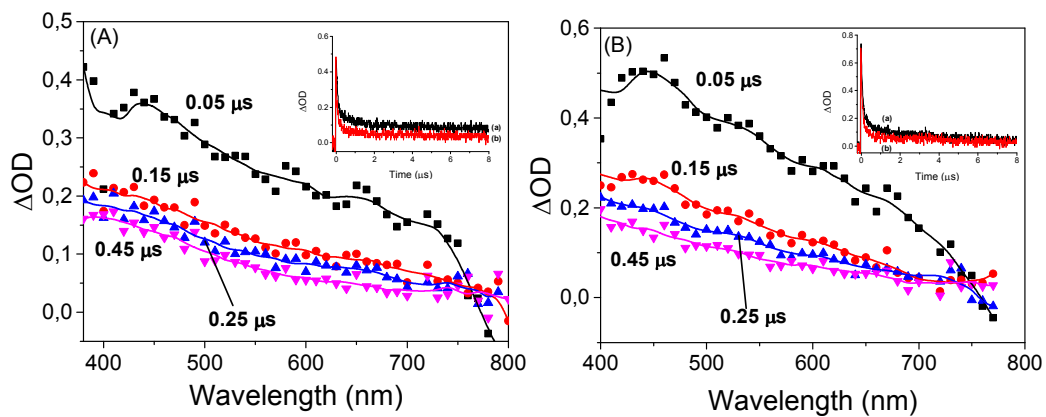


Fig. 12.

